Supporting Information for:

Multiconfigurational photodynamics simulations reveal the mechanism of photodecarbonylation reactions of cyclopropenones in explicit aqueous environments.

Authors list: Daniel M. Adrion, Waruni V. Karunaratne, and Steven A. Lopez*

Department of Chemistry and Chemical Biology, Northeastern University, Boston, Massachusetts, 02115, United States

We have uploaded all optimized critical points, initial conditions for the non-adiabatic molecular dynamics (NAMD) for gas-phase and solvated dynamics, and the data obtained from the respective dynamics simulations in a zipped folder here on Figshare (DOI: 10.6084/m9.figshare.21667808).

Figure S1 shows the (10,9) active space used for all multiconfigurational calculations performed on **1**. These orbitals and their occupations were calculated at the SA(4)-XMS-CASPT2/ANO-S-VDZP//SA(4)-CASSCF(10,9)/ANO-S-VDZP level of theory.

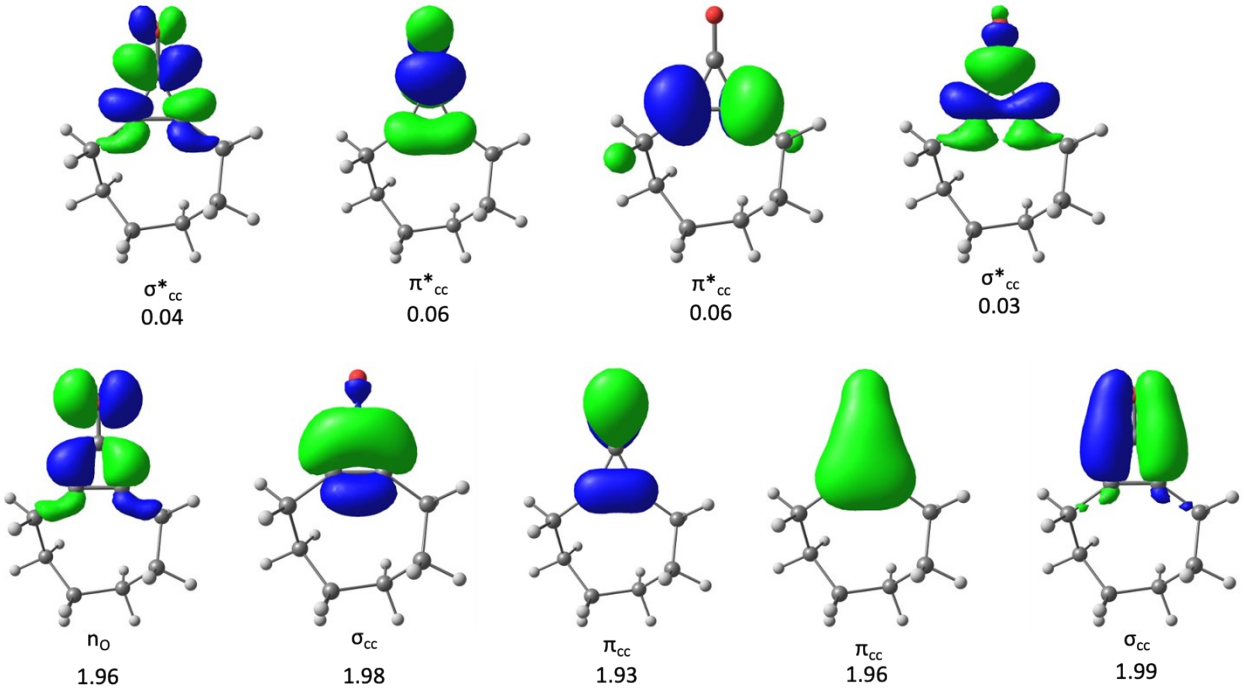

Figure S1. CASSCF(10,9) active space for the global minimum of **1** with average occupation numbers. The orbitals were calculated using SA(4)-XMS-CASPT2/ANO-S-VDZP//SA(4)-CASSCF(10,9)/ANO-S-VDZP. The orbitals were generated with a contour value of 0.06.

To determine the local environment around the Franck-Condon (FC) hopping points of **2**, we characterized the topology (branching space) of an MECI for **2** (**2-MECI**) located in the FC region of the hopping seam (Figure S2). We also visualized the non-adiabatic coupling (*h*) and gradient (*g*) vectors of the hopping point geometry (Figure S2b).

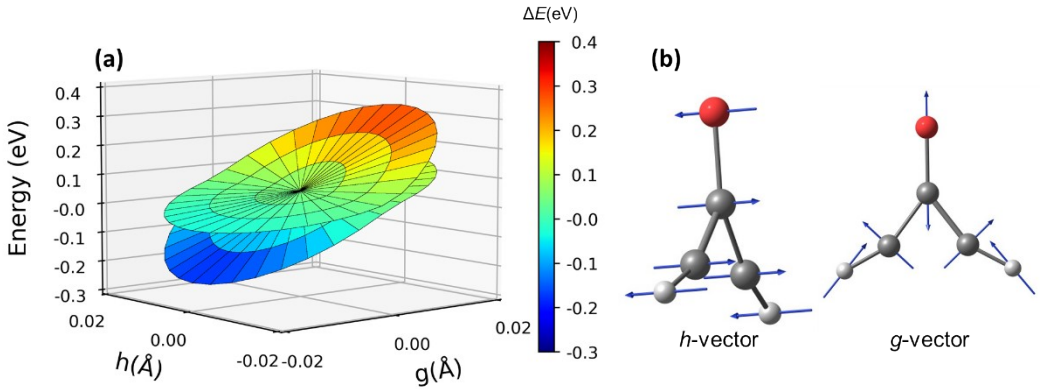

Figure S2. The branching plane of **2-MECI** visualized over the *g* and *h*-vector space (a) and the *g* and *h*-vectors of **2-MECI** (b). The blue arrows represent the positive directions of vibration.

The PES around **2-MECI** has a sloped topology and follows a single relaxation path toward the ground state in the negative direction of the *g*-vector. The vibrations corresponding to the *g* and *h*-vectors (Figure S2b) correspond to an out-of-plane vibration for the cyclopropenone ring (*h*-vector) and a reversion towards the cyclopropenone reactant (*g*-vector). The vectors and branching space of **2-MECI** suggest that **2** will revert to cyclopropenone after crossing to the S_0. Next, we will analyze hopping point geometries corresponding to concerted C-C bond dissociation mechanisms for the gas-phase NAMD simulations of **1**. These geometries ($\mathbf{1}_{\mathbf{conc\text{-}1}}$ and $\mathbf{1}_{\mathbf{conc\text{-}2}}$) are shown in Figure S3. The σ_{CC} bond distances at these points are 1.88 Å/1.76 Å ($\mathbf{1}_{\mathbf{conc\text{-}1}}$) and 1.91 Å/1.81 Å ($\mathbf{1}_{\mathbf{conc\text{-}2}}$), all of which correspond to broken σ_{CC} bonds. Both trajectories form the dissociation product, as indicated by the pathways after the hopping points (main text Figure 5).

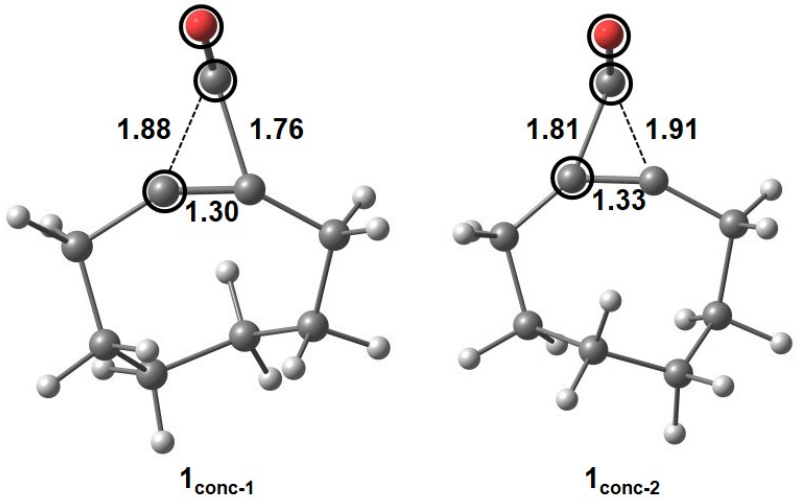

Figure S3. S_1/S_0 hopping point geometries corresponding to the concerted mechanism pathways (difference of less than 0.25 Å for the σ_{CC} bonds in the ring).

The O-C-C angles (atoms circled in black in Figure S3) are 120° ($\mathbf{1}_{\mathbf{conc\text{-}1}}$) and 108° ($\mathbf{1}_{\mathbf{conc\text{-}2}}$). These large deviations from planarity suggest that the $C_{carbonyl}$ atom becomes significantly more pyramidalized in these structures than in the reactant. The C=C bonds in $\mathbf{1}_{\mathbf{conc\text{-}1}}$ and $\mathbf{1}_{\mathbf{conc\text{-}2}}$ are

slightly shorter than in the optimized S_0 minimum geometry (1.35 Å), which suggests there is more double bond character at these hopping point geometries across the methylene bond than in the S_0 minimum. The C=O bonds in the cyclopropenone rings of $\mathbf{1}_{\mathbf{conc\text{-}1}}$ (1.13 Å) and $\mathbf{1}_{\mathbf{conc\text{-}2}}$ (1.14 Å) are also significantly shorter than the corresponding bond in the S_0 minimum (1.18 Å). This bond contraction suggests that concerted hopping points geometries are heavily predistorted towards the dissociation products (CO and cyclooctyne) due to the contraction of both the C=O and C=C methylene bonds as the concerted hopping point geometries are approached. To understand how the σ_{CC} bond distances at the hopping point geometries affect the outcome of the reaction, we plotted the ratio of dissociating trajectories for a given range of σ_{CC} bonds in the cyclopropenone rings of **1** and **2**.

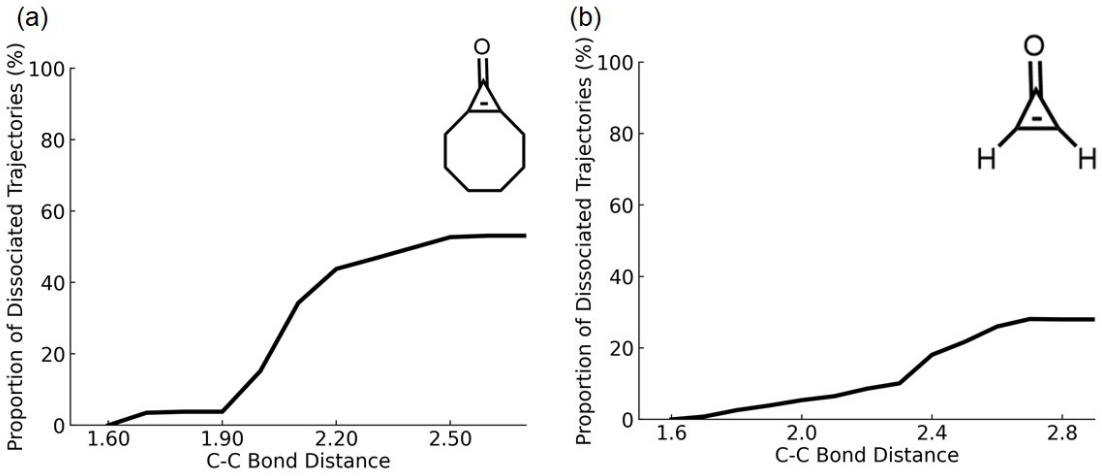

Figure S4. Plots depicting the proportion of trajectories crossing through S_1/S_0 hopping point geometries at given bond lengths. Bond length ranges of 1.60 - 2.50 Å and 1.60 - 2.80 Å were used for **1** and **2**, respectively.

To determine if there was an inflection point for either **1** or **2**, we calculated the proportion of trajectories that dissociated at a given bond length. The x-axes on the plots represent the longer of the σ_{CC} bond lengths in the cyclopropenone ring at the hopping geometry, and the y-axis on the plots represents the ratio of trajectories that ultimately dissociated after going through that hopping point. For both **1** and **2**, we started at a bond distance of 1.60 Å, where both σ_{CC} bonds are fully intact. For **1**, we observe marginal increases in the quantum yield of dissociation up through 1.90 Å and a sharp increase when going from 1.90 Å (4% of trajectories dissociated) through 2.20 Å (44% trajectories undergoing dissociation), and then steadily approaching the quantum yield. We observe a similar pattern for **2**, which has a much smaller inflection point between 2.30 Å (11% of trajectories dissociated) and 2.40 Å (18% of trajectories dissociated). After this, the proportion steadily increases until it approaches the calculated quantum yield for the reaction (28%). The proportion of dissociated trajectories asymptotically approach the quantum yield for the respective simulations of 53% (**1**) and 28% (**2**) as the maximum σ_{CC} bond distance from a hopping point is approached. The longest σ_{CC} bond bond distance recorded for a hopping point along the seam for **1** was 2.58 Å, and the longest σ_{CC} bond distance for **2** had was 2.77 Å. Because of this, we terminated the analysis of the bond lengths at 2.60 Å and 2.80 Å for **1** and **2**, respectively. Next,

we assessed the excited state lifetimes for **1** and **2** calculated from both the gas-phase and solvated NAMD simulations.

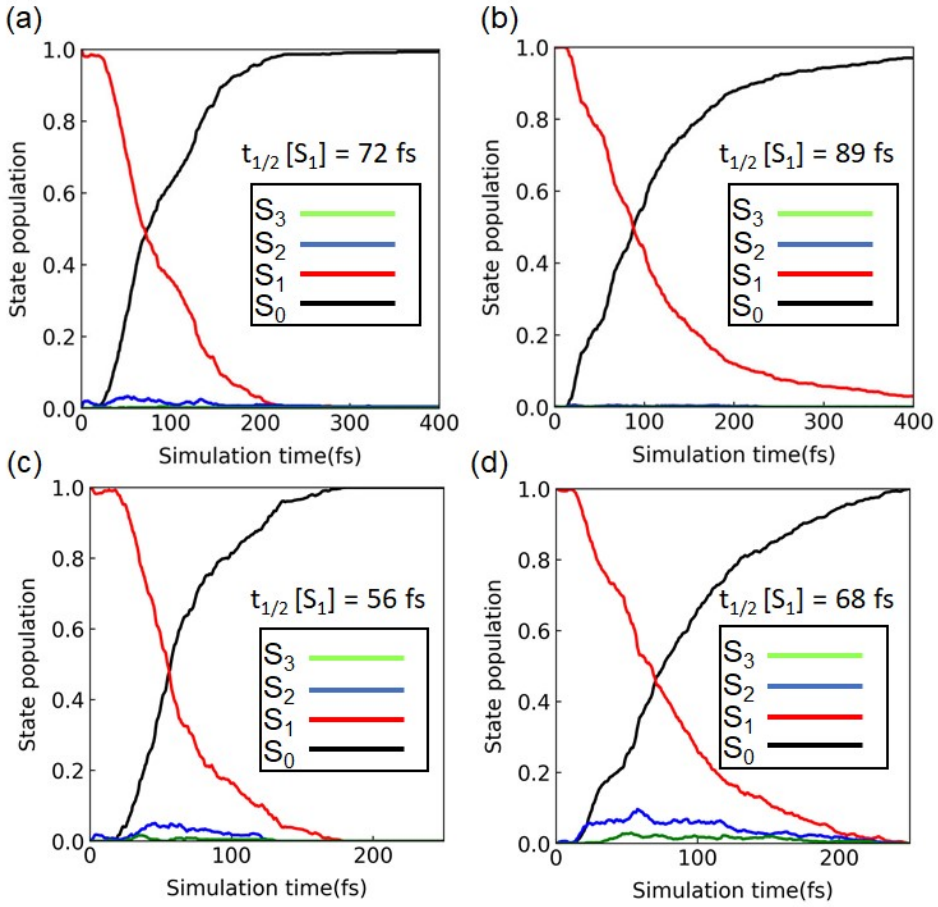

Figure S5. Plots of the state population for the S_0 and first three excited states of **1** in the gas-phase(a) and solvated phase (c) and **2** in the gas-phase (b) and solvated phase (d). The excited-state lifetime plots show the first 400 fs of the gas-phase dynamics, and 250 fs for the solvated dynamics trajectories.

Figure S5 shows the $S_{0\text{-}3}$ state populations for **1** and **2** for the gas-phase and solvated dynamics simulations. All four plots suggests that ultrafast decay from the S_1 to the S_0 will in the presence or absence of solvent (water). We computed S_1 lifetimes ($t_{1/2}$) of 72 and 89 fs for **1** and **2** in the gas-phase, and 56 and 68 fs for **1** and **2** in the solvent shells. The S_1 lifetimes were significantly shorter in the solvent simulations than in the gas-phase (16 fs shorter for **1** and 21 fs shorter for **2**), indicating that the S_1/S_0 hopping seams were more accessible when water was added to the systems. The state populations of the S_2 and S_3 states remained negligibly small throughout the course of all trajectory simulations (<10% total population). We also observed a longer S_1 lifetime for **2** over **1** for both the gas-phase and solvent phases (17 fs longer and 12 fs longer, respectively). This is consistent with the results obtained from both the static (MEP) and dynamic (NAMD) calculations, which showed that the unsubstituted cyclopropenone will preferentially go towards

and S_1 minimum and fluoresce down to the S_0 state, while the COT-precursor will propagate towards an S_1/S_0 hopping region after initial excitation.

In addition to running calculations using CASSCF(10,9), we have computed the vertical excitation energies and transitions using two additional active space: CASSCF(12,10) and CASSCF(8,8). The orbitals and their average occupancies for the optimized ground state minimum of **2** are shown below in Figure S6. We also show the vertical excitation energies and transition natures for both active spaces for both **1** and **2** in Tables S1 and S2, respectively. The (8,8) active space was produced by removing one of the σ_{CC} orbitals from the set of 5 occupied orbitals, and the (12,10) active space was generated by including an additional σ_{CO} orbital to the (10,9) active space.

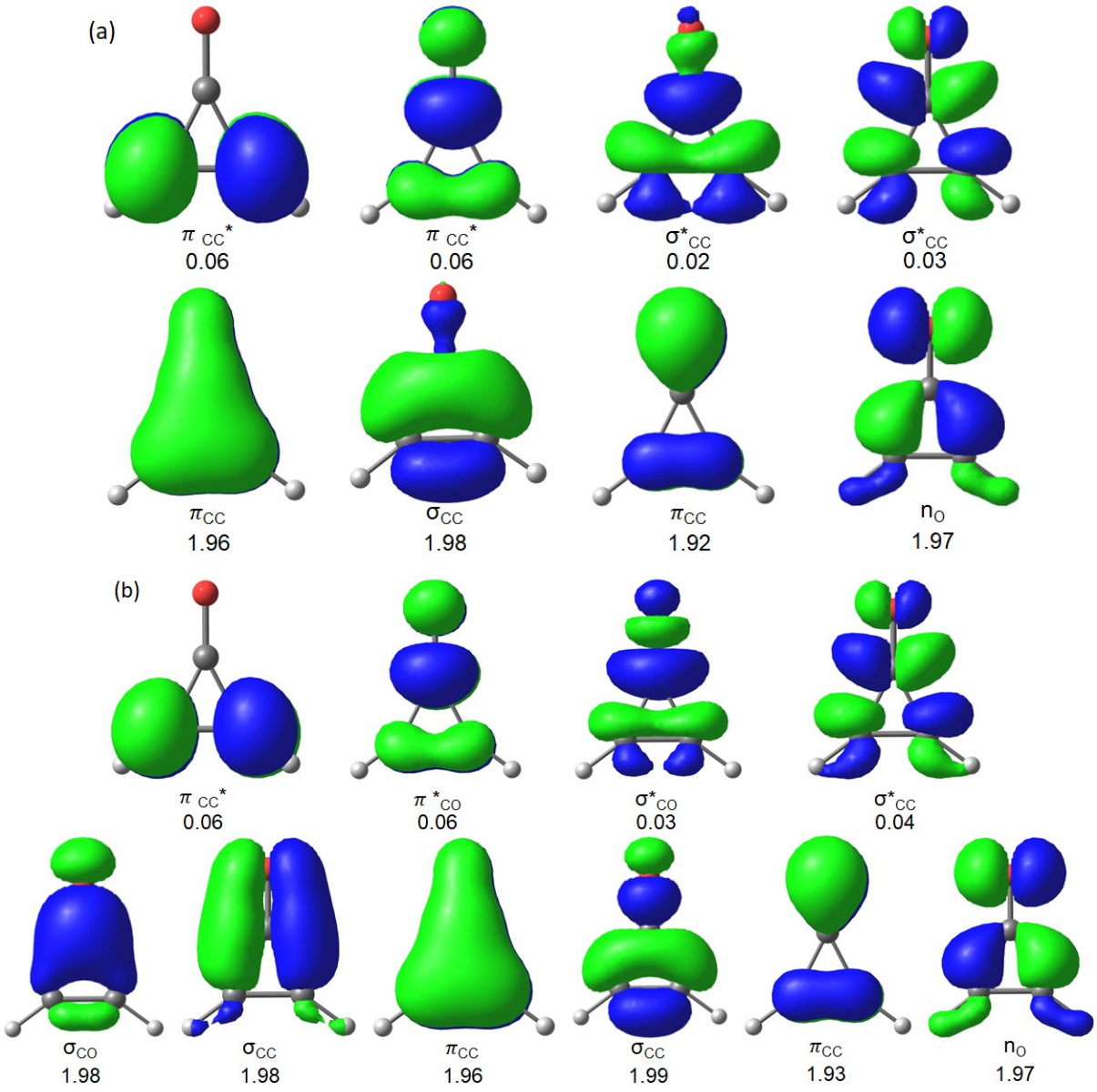

Figure S6. Active spaces for **2** computed using SA(4)-CASSCF(8,8)/ANO-S-VDZP (a) and SA(4)-CASSCF(12,10)/ANO-S-VDZP (b) levels of theory. The average orbital occupations for

the S_0 minimum geometries are given below their respective orbitals. The (12,10) and (8,8) active spaces for **1** include the same orbitals.

Table S1. Excitations to the first three excited states of **1** and **2** calculated using SA(4)-XMS-CASPT2//SA(4)-CASSCF(8,8)/ANO-S-VDZP. Energies are presented in eV, and the oscillator strengths of each transition are also given.

Molecule	State	Energy (eV)	Wavelength (nm)	Oscillator strength	Nature
1	S_1	4.98	249	0.0089	$n_O \rightarrow \pi^*$ (S_1)
	S_2	5.66	219	0.0000	$n_O \rightarrow \pi^*$ (S_2)
	S_3	7.42	167	0.0838	$\pi \rightarrow$ Ryd (S_3)
2	S_1	4.29	289	0.0063	$n_O \rightarrow \pi^*$(S_1)
	S_2	5.41	229	0.0000	$n_O \rightarrow \pi^*$ (S_2)
	S_3	7.12	174	0.0529	$\pi \rightarrow \pi^*$ (S_3)

Table S2. Excitations to the first three excited states of **1** and **2** calculated using SA(4)-XMS-CASPT2//SA(4)-CASSCF(12,10)/ANO-S-VDZP. Energies are presented in eV, and the oscillator strengths of each transition are also given.

Molecule	State	Energy (eV)	Wavelength (nm)	Oscillator strength	Nature
1	S_1	4.87	255	0.0097	$n_O \rightarrow \pi^*$ (S_1)
	S_2	5.43	228	0.0000	$n_O \rightarrow \pi^*$ (S_2)
	S_3	7.22	172	0.0969	$\pi \rightarrow$ Ryd (S_3)
2	S_1	4.41	281	0.0070	$n_O \rightarrow \pi^*$(S_1)
	S_2	5.55	223	0.0000	$n_O \rightarrow \pi^*$ (S_2)
	S_3	6.99	177	0.0660	$\pi \rightarrow \pi^*$ (S_3)

Conformational sampling and analysis of 1: Before performing calculations to evaluate the photodissociation mechanism of cyclopropenone, we first performed a conformational search for **1** using the Conformer-Rotomer Ensemble Sampling Tool (CREST) software, which uses metadynamics simulations to sample the conformational space of molecules (DOI: 10.1039/C9CP06869D). All conformers obtained from CREST were re-optimized with PBE0-D3BJ/cc-pVDZ. The conformational search yielded five conformers with a free-energy (ΔG) range of 0-4.4 kcal mol^{-1}. The structures of all these conformers are shown in Figure S7.

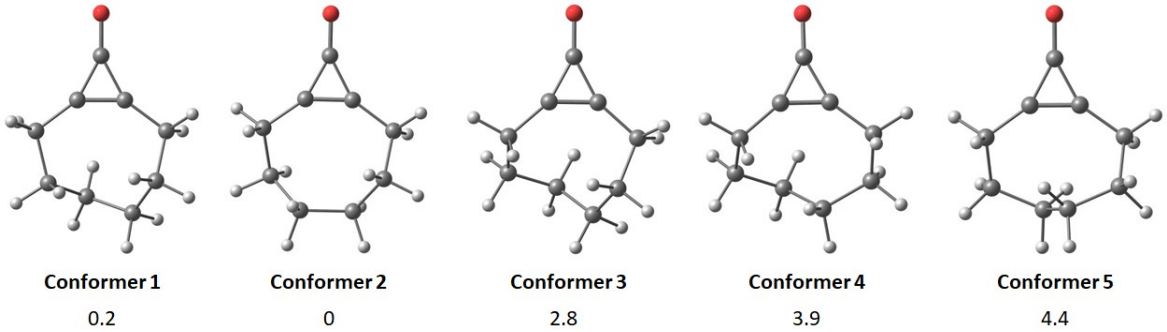

Figure S7. Ground-state conformers of **1** obtained from a conformational search using CREST. Energies are presented in kcal mol^{-1}.

The conformational search of **1** on the ground state yielded 5 distinct local minima, with an energy range of 4.4 kcal mol^{-1}. There are two low-energy conformers (0 and 0.2 kcal mol^{-1}), and 3 high-energy conformers (ΔG values of 2.8, 3.9, and 4.4 kcal mol^{-1}, respectively). Based on the nearly degenerate energies of conformers 1 and 2, we predict that **1** will rapidly interconvert between these two structures, while the other structures will be present in negligible ratios (we calculate that the ratios between conformer 1 and conformers 3, 4, and 5 will be approximately 100:1, 500:1, and 2000:1, respectively. Below, we show two overlays of the SA(4)-CASSCF(10,9)/ANO-S-VDZP optimized with conformer 1 (left) and conformer 2 (right).

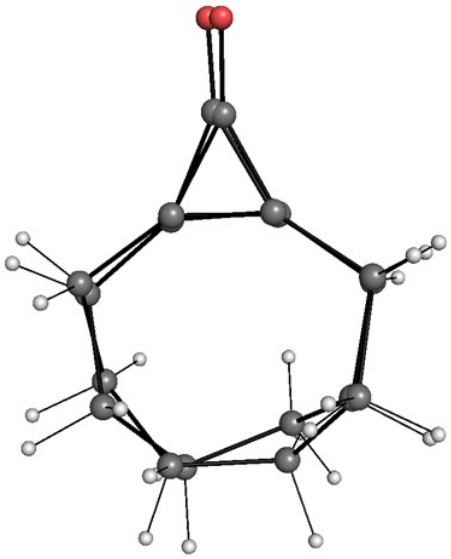

Figure S8. Overlay of CASSCF optimized S_0 minimum with low energy conformers obtained from CREST for the cyclooctyne-precursor (**1**). The CREST conformers were optimized with PBE0-D3BJ/cc-pVDZ.

The CASSCF-optimized conformer resembles a mirror image of conformer 1 compared to conformer 2. To determine if the initial configuration on the ground state significantly affects the photochemical reactivity, we sampled a Wigner ensemble of geometries for conformer 2 (the global minimum found from CREST), and ran dynamics from the Franck-Condon (FC) region on the S_1 PES. Our results obtained from the dynamics simulations are presented below. We observed a large energy range (90.4 kcal/mol) according to CAS(10,9)/ANO-S-VDZP for the Wigner-

sampled geometries. All conformers found using CREST are well within the energy range of the Wigner-sampled conformers.

To evaluate the effects of state averaging on the photochemistry of **2**, we ran 500 NAMD simulations for 1 ps with a 0.5 fs time step using SA(2). These simulations had the same calculation parameters as the SA(4) simulations with fewer states considered. We plotted the breaking C-C σ bonds in the cyclopropenone ring over the course of the full ps, and the results are presented in the figure below. The black dots represent the S_1/S_0 hopping seam.

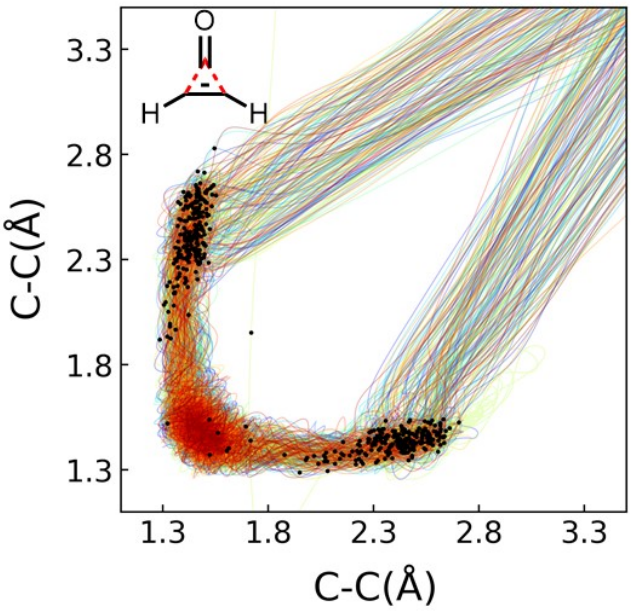

Figure S9. Trajectory bond dissociation plot for **2** calculated using SA(2). The pathways represent the C-C σ bond lengths in the ring (depicted with the red dotted lines), and the black dots represent the S_1/S_0 surface hopping points.

Figure S9 shows the C-C bonds in the cyclopropenone ring plotted over the course of a 1 ps trajectory run using SA(2)-CASSCF(10,9)/ANO-S-VDZP. The bond dissociation in Figure S7 is consistent with Figure 4b in the manuscript showing the SA(4)-CASSCF/ANO-S-VDZP dynamics results. These figures both show that the photochemical mechanism is an asynchronous process where one C-C bond in the cyclopropenone ring breaks on the S_1 state, and the other breaks on the S_0 state. One significant difference between the dynamics simulations run with SA(4)-CASSCF/ANO-S-VDZP and SA(2)-CASSCF/ANO-S-VDZP is the number of points in the asynchronous and FC regions. When running the dynamics using SA(4)-CASSCF/ANO-S-VDZP, the percentage of trajectories that passed through a hopping point in the asynchronous region for **2** was 28% compared to 72% passing through a hopping point in the FC region. This is different for the SA(2)-CASSCF(10,9)/ANO-S-VDZP dynamics, where just 8 trajectories total pass through a hopping point in the FC region (2%), compared to the other 98% of trajectories that cross through a hopping point in the asynchronous region of the seam. The Φ for the two methods was also significantly different. For the SA(4)-CASSCF(10,9)/ANO-S-VDZP and SA(2)-CASSCF(10,9)/ANO-S-VDZP dynamics simulations, the total Φ of decarbonylation was 28% and

73%, respectively. We hypothesize that this nearly threefold difference in yield is due to the pathway towards the S_1 minimum not being accessible for the SA(2)-CASSCF(10,9)/ANO-S-VDZP dynamics. The S_2 and S_3 states (corresponding to π – π* excitations according to our vertical excitation energy calculations with both DFT and CASSCF) are not considered. This leaves only the n – π* excitation to be accessed for the SA(2)-CASSCF(10,9)/ANO-S-VDZP dynamics and becomes the preferred decarbonylation pathway, a result which is inconsistent with experiment. Because of these reasons, we believe that the need to include at least one ππ* state in the multiconfigurational calculations.

Table S3. Dynamics simulations results for gas-phase dynamics simulations of **1** and **2**. All simulations were run from the S_1 Franck-Condon region of the PES. 500 Initial conditions sampled by an S_0 Wigner distribution. All trajectories were run using SA(4)-CASSCF/ANO-S-VDZP.

Molecule	Trajectories ending on S_0	Product yield (%)	Reactant yield (%)
1	429	53	47
2	464	28	72

Table S4. Dynamics simulations results for implicitly solvated dynamics simulations of **1** and **2**. All simulations were run from the S_1 Franck-Condon region of the PES. 500 Initial conditions sampled by an S_0 Wigner distribution. All trajectories were run using SA(4)-CASSCF(10,9)/ANO-S-VDZP.

Molecule	Trajectories ending on S_0	Product yield (%)	Reactant yield (%)
1	495	57	43
2	492	37	63

Table S5. Dynamics simulation results for explicitly solvated dynamics simulations of **1** and **2**. All simulations were run from the S_1 Franck-Condon region of the PES. 500 Initial conditions sampled by an S_0 Wigner distribution. All trajectories were run using SA(4)-CASSCF(10,9)//ANO-S-VDZP.

Molecule	Trajectories ending on S_0	Product yield (%)	Reactant yield (%)
1	253	58	42
2	461	58	42

Table S6. Dynamics simulations results for explicitly solvated QM/MM dynamics simulations of **1** and **2**. All simulations were run from the S_1 Franck-Condon region of the PES. 500 Initial conditions sampled by an S_0 Wigner distribution. All trajectories were run using SA(4)-CASSCF(10,9)//ANO-S-VDZP.

Molecule	Trajectories ending on S_0	Product yield (%)	Reactant yield (%)
1	460	53	47
2	441	75	25

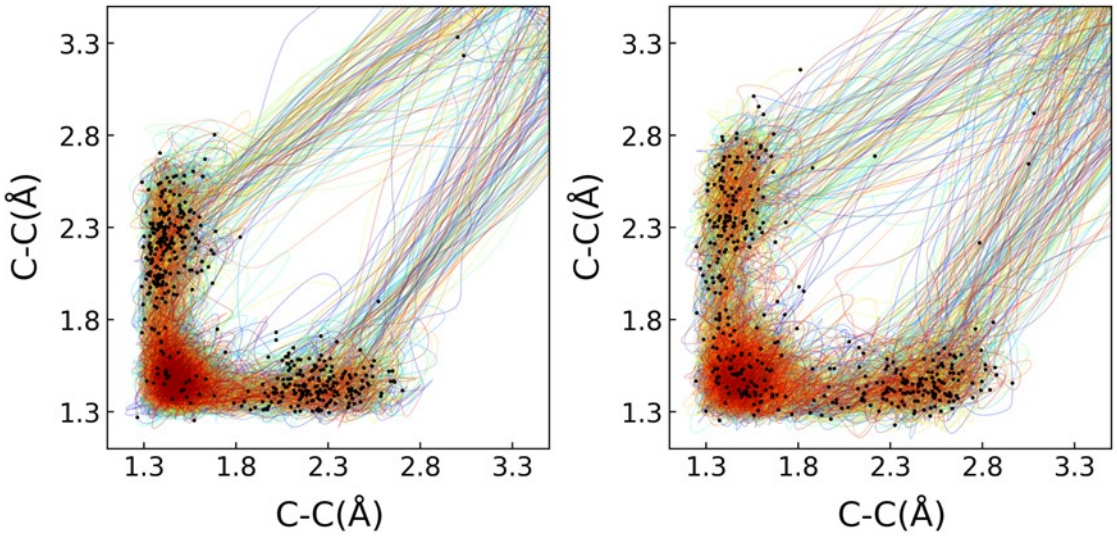

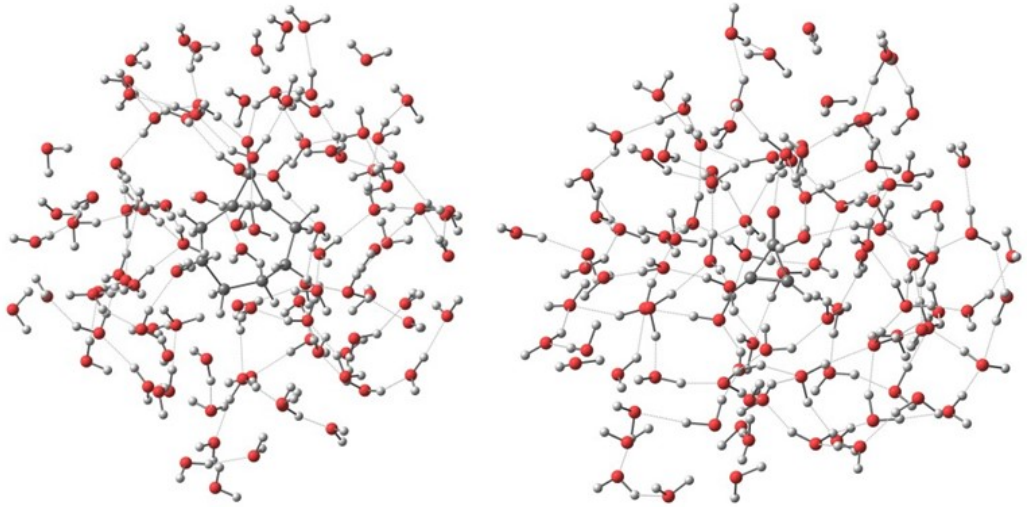

Figure S10. Bond dissociation plots for **1** (left) and **2** (right) for NAMD simulations using QM/MM. The QM method on the chromophore was SA(4)-CASSCF/ANO-S-VDZP and the MM method used an SPC forcefield for water. We also show representative structures of the chromophores solvated with 100 water molecules under each plot.

We generated 500 Wigner-sampled structures from the S_0 minimum of **1** and **2** and ran 0.5 ps NAMD simulations using an implicit solvent model for water (PCM model[1, 2]). To compare the effects of using an implicit solvent model to running gas-phase NAMD simulations, we computed the Φ for the decarbonylation reaction and the ratios of hopping points that went through the asynchronous and Franck-Condon regions for both classes of simulations. For the gas-phase NAMD simulations, the Φ for the dissociation of **1** and **2** was 0.53 and 0.28, respectively. For the implicitly solvated simulations, the same values were 0.57 and 0.37, respectively. We observe a slight increase in the dissociation rate while using the implicit solvent model, but the results are still qualitatively in agreement with experimental results.

References

(1) Cossi, V. B. a. M. Quantum Calculation of Molecular Energies and Energy Gradients in Solution by a Conductor Solvent Model. *J. Phys. Chem.* **1998**, *102*, 1995-2001.
(2) Maurizio Cossi, N. R., Giovanni Scalmani, and Vincenzo Barone. Polarizable dielectric model of solvation with inclusion of charge penetration effects. *J. Chem. Phys.* **2001**, *114* (5691). DOI: 10.1063/1.1354187#.